JOURNAL OF COMPUTATIONAL PHYSICS 67, 59 72 (1986)

An Implicit Monte Carlo Scheme for Calculating Time-Dependent Line Transport*

E. D. BROOKS III AND J. A. FLECK, JR.

University of California, Lawrence Livermore National Laboratory
Livermore, California 94550

Received October 11, 1985; revised January 10, 1986

We have developed an implicit Monte Carlo technique for describing time-dependent line transport in the presence of collisional coupling between atomic levels. The method is applied to the time-dependent description of a two-level system in plane parallel slab geometry. For a set of test problems the stability of the scheme is independent of the choice of time-step, indicating the robustness of the method. The method is shown to be applicable to both optically thin and opticaly thick media. © 1986 Academic Press, Inc.

1. INTRODUCTION

The transport of radiation from resonance lines is important in the study of stellar atmospheres [1] and laser produced plasmas [2]. The trapping of resonance radiation in vapors is important in a variety of experimental situations, although it is frequently regarded as an unwanted complication. This phenomenon has been studied both theoretically [3 5] and experimentally. The experiments may be regarded as either steady state [6, 7] or time dependent [8].

Most of the methods devised thus far for computing line transport have been restricted to steady state applications. (See [1] and the references therein.) Linearized treatments of two-level time-dependent line transport have been developed by Kunasz [9] and Alley [10]. To our knowledge, however, no method applicable to nonlinear time-dependent line transport with collisions has yet been published. In this paper we describe a Monte Carlo method for solving such problems for two-level systems, which is capable of generalization to more levels. The generalization to more levels will be treated in a later publication.

The Monte Carlo method has several advantages over the more conventional discrete ordinate methods. In multidimensional geometry, where the need for adequate sampling in frequency, direction, and space becomes particularly onerous for discrete ordinate methods, the Monte Carlo method has a distinct advantage. Com-

* Work performed under the auspices of the U. S. Department of Energy by the Lawrence Livermore National Laboratory under Contract W-7405-ENG 48.

0021-9991/86 $3.00

plex scattering effects such as partial frequency redistribution are also handled with greater ease using Monte Carlo [11, 12].

The main defect of the Monte Carlo method is the statistical variation in the estimate of the radiation intensity. On the other hand the level of fluctuation of atomic state populations can be quite acceptable, since these depend on integrals over the radiation field and are consequently smoother than the radiation intensity itself.

The basic difficulty underlying the numerical solution of the coupled time-dependent level population and radiative transfer equations is that they constitute a stiff system. Thus the time differencing scheme must be implicit in all of the dependent variables to ensure stability. When this is accomplished, time integration steps can be selected on the basis of acceptable changes per step in the physical variables rather than on stability conditions.

An implicit Monte Carlo method was developed earlier for solving the time dependent radiation transport and material energy equations under LTE conditions [13, 14]. The basic step in the derivation of the method is to write the material energy conservation equation as an implicit difference equation. With this equation one can express the source term in terms of an integral of the specific intensity over direction and frequency. Substitution of the source term in this form into the radiation transport equation is formally equivalent to the introduction of a scattering process representing the absorption and reemission of radiation. The remaining absorption coefficient and the scattering coefficient for the new process together add up to the absorption coefficient in the original transport equation. The larger the integration time-step and/or the local Planck mean absorption coefficient, the larger the contribution of scattering. The implicit Monte Carlo method has been empirically demonstrated to be unconditionally stable for certain simple equation of state and opacity models [13].

The problem of two-level line transport can be treated analogously. One writes the rate equation for the upper level, including both collisions and radiative transitions as an implicit difference equation. This equation can be used to express the spontaneous emission source in the radiation transport equation in terms of an integral of the radiation field over direction and frequency. As in the LTE case the presence of this integral in the source term corresponds to a scattering process. The original absorption coefficient is divided into absorption and scattering contributions with the scattering contribution becoming more important as the time integration step increases.

In this paper we shall consider for simplicity slab geometry and complete frequency redistribution in the scattering, since our primary interest is in demonstrating the stability and accuracy of the implicit Monte Carlo scheme for line transport applications. Generalization to more complex geometries and scattering models is straightforward.

The outline of the paper is as follows. In Section 2 we derive the basic equations used in the method. The derivation of the atomic population equations and the transfer equation, which includes effective scattering terms, closely parallels the

derivation for the LTE case [13]. In Section 3 we describe the Monte Carlo procedure used to solve the equations derived in Section 2. Numerical results are described in Sections 4 and 5. Computation times are discussed in Section 6, and conclusions are contained in Section 7.

2. The Mathematical Method

The radiation transport equation for a two-level system in slab geometry is

$$\frac{\partial f}{\partial t}+\mu c\frac{\partial f}{\partial x}=\frac{n_2}{2}A_{21}\phi-c(K_{12}n_1-K_{21}n_2)\phi f, \tag{2.1}$$

where c is the speed of light, x is the position in the slab, μ is the direction cosine of the radiation, ν is the frequency of the radiation, $f(\mu, \nu, x, t)$ is the photon number density distribution per unit atom density, $n_2(x, t)$ is the upper level population fraction, $n_1(x, t)$ is the lower level population fraction, A_{21} is the spontaneous emission rate, $\phi(\nu)$ is the normalized line shape function for absorption and $K_{12}=\kappa N$, where κ is the lower state absorption cross section and N is the atom number density. The coefficient K_{21} is defined by

$$K_{21}=\frac{g_1}{g_2}K_{12}, \tag{2.2}$$

where g_1 and g_2 are the usual statistical weight factors for levels 1 and 2.

The equations governing the atomic population fractions n_1 and n_2 are

$$\frac{dn_2}{dt}=C_{12}n_1-C_{21}n_2-A_{21}n_2+c(K_{12}n_1-K_{21}n_2)\int_1^{-1}d\mu\int_0^{\infty}d\nu\,\phi(\nu)f(\mu,\nu) \tag{2.3}$$

and

$$n_1+n_2=1, \tag{2.4}$$

where C_{12} and C_{21} are rate contants for the collisional transitions $1\to 2$ and $2\to 1$, respectively.

Using (2.4) one can rewrite (2.1) and (2.3) as

$$\frac{\partial f}{\partial t}+\mu c\frac{\partial f}{\partial x}=\frac{n}{2}A_{21}\phi-c[K_{12}-(K_{21}+K_{12})n]\phi f \tag{2.5}$$

and

$$\frac{dn}{dt}=C_{12}-(C_{12}+C_{21}+A_{21})n+c[K_{12}-(K_{21}+K_{12})n]\int_1^{-1}d\mu\int_0^{\infty}d\nu\,\phi(\nu)f(\mu,\nu), \tag{2.6}$$

respectively, where n is the upper level population fraction.

We now turn to creating a scheme for solving these equations numerically. Following the implicit Monte Carlo technique as described in [13], we derive a finite difference solution for (2.6) using semiimplicit differencing. To generate a prescription for obtaining $n(t_0+\Delta t_n)$ from $n(t_0)$ we integrate (2.6) from t_0 to $t_0+\Delta t_n$. If we approximate $n(t)$ by $n(t_0+\Delta t_n)$ in the spontaneous emission and collision terms and $n(t_0)$ in the absorption term, we obtain

$$n(t_0+\Delta t_n)=n(t_0)+[C_{12}-(C_{12}+C_{21}+A_{21})]\,n(t_0+\Delta t_n)\,\Delta t_n + c[K_{12}-(K_{21}+K_{12})\,n(t_0)]\int_{t_0}^{t_0+\Delta t_n} dt\int_{-1}^{1} d\mu\int_{0}^{\infty} dv\phi(v)f(\mu, v, t). \tag{2.7}$$

Note that we have treated the term involving time constants implicitly and the net absorption term explicitly. Implicit time centering has been used on the terms most likely to affect stability. Use of explicit time centering for the net absorption term is unlikely to affect stability and also brings about great simplification. Solving (2.7) for $n(t_0+\Delta t_n)$ gives

$$n(t_0+\Delta t_n)=\gamma n(t_0)+\gamma\Delta t_n C_{12}+\gamma c[K_{12}-(K_{21}+K_{12})\,n(t_0)] \times\int_{t_0}^{t_0+\Delta t_n} dt\int_{-1}^{1} d\mu\int_{0}^{\infty} dv\,\phi(v)f(\mu, v, t), \tag{2.8}$$

where γ is defined by

$$\gamma=\frac{1}{1+\Delta t_n(C_{12}+C_{21}+A_{21})}. \tag{2.9}$$

Equation (2.8) gives us a prescription for finding $n(t_0+\Delta t_n)$ given $n(t_0)$ and the history of the radiation field over the time interval.

We now need a transport equation for the radiation field between the times t_0 and $t_0+\Delta t_n$ which is consistent with (2.8). To derive this equation we consider a finite difference solution for $f(t)$ between the times t_0 and $t_0+\Delta t_n$ with a possibly smaller step size Δt_f. We denote the sequence of time-steps between t_0 and $t_0+\Delta t_n$ by t_i. Integrating (2.5) from t_i to $t_i+\Delta t_f$ and for simplicity dropping the $\partial/\partial x$ term which is not germane to this discussion, we obtain

$$f(t_i+\Delta t_f)=f(t_i)+\frac{A_{21}\phi}{2}\int_{t_i}^{t_i+\Delta t_f} dt\,n(t)+c\phi\int_{t_i}^{t_i+\Delta t_f} dt[(K_{12}+K_{21})\,n(t)-K_{12}]f(t). \tag{2.10}$$

Now we must choose the approximations which we will use for $n(t)$ and $f(t)$ in the time integrals. If Δt_f were equal to Δt_n, then consistency with the implicit differencing of (2.7) would demand that we substitute $n(t_0+\Delta t_n)$ for $n(t)$ in the

spontaneous emission term and $n(t_0)$ for $n(t)$ in the absorption term. Making use of these substitutions and (2.8), we obtain for (2.10) the form

$$f(t_i+\Delta t_f)=f(t_i)+\frac{A_{21}\phi}{2}\int_{t_i}^{t_i+\Delta t_f} dt\Big\{\gamma n(t_0)+\gamma\Delta t_n C_{12}+\gamma c[K_{12}-(K_{21}+K_{12})\,n(t_0)]$$
$$\times\int_{-1}^{1} d\mu\int_0^{\infty} dv\,\phi(v)\int_{t_0}^{t_0+\Delta t_n} d\tau f(\mu, v, \tau)\Big\}$$
$$-c\phi[K_{12}-(K_{12}+K_{21})\,n(t_0)]\int_{t_i}^{t_i+\Delta t_f} dt\,f(t). \tag{2.11}$$

If $\Delta t_f<\Delta t_n$ the substitution of $n(t_0+\Delta t_n)$ for $n(t)$ requires knowledge of $f(t)$ for times exceeding $t_i+\Delta t_f$ to compute $f(t_i+\Delta t_f)$. To avoid this problem we approximate the time integral over τ by $\Delta t_n f(\mu, v, t)$. Equation (2.11) gives us a prescription for computing $f(t)$ in the interval from t_0 to $t_0+\Delta t_n$. Taking the limit $\Delta t_f\to 0$, we obtain a differential equation for $f(t)$ between the time steps of the solution for $n(t)$. If we now include the spatial derivatives which were dropped for the above discussion, we obtain

$$\frac{\partial f}{\partial t}+\mu c\frac{\partial f}{\partial x}=\frac{\gamma A_{21}\phi}{2}[n(t_0)+\Delta t_n C_{12}]+\frac{\gamma c A_{21}\phi\Delta t_n}{2}\Big\{[K_{12}-(K_{21}+K_{12})\,n(t_0)]$$
$$\times\int_{-1}^{1} d\mu\int_0^{\infty} dv\,\phi(v)f(\mu, v)\Big\}-c\phi[K_{12}-(K_{12}+K_{21})\,n(t_0)]f. \tag{2.12}$$

Equation (2.12) can also be justified in the following way. Consider the differencing of (2.5) and (2.6) with respect to time in which the dependent variables are all implicit with the exception of $n(t)$ in the absorption terms, which is left explicit. The resulting difference equations can be combined to give a single difference equation that involves only the radiation distributon. This difference equation will be identical to the one obtained by differencing (2.12) with respect to time and keeping the radiation distribution implicit. Thus a Monte Carlo solution of (2.12) should be consistent with the solution to the implicit finite difference approximations of (2.5) and (2.6).

Examination of (2.12) shows that the net absorption coefficient

$$\sigma(v)=\phi(v)[K_{12}-(K_{21}+K_{12})\,n(t_0)] \tag{2.13}$$

is now divided into an absorption contribution

$$\sigma_a(v)=\hat{f}\sigma(v) \tag{2.14}$$

and a scattering contribution

$$\sigma_s(v)=(1-\hat{f})\,\sigma(v), \tag{2.15}$$

where the fraction $\hat{f}$ is given by

$$\hat{f}=\frac{1+\Delta t_n(C_{12}+C_{21})}{1+\Delta t_n(C_{12}+C_{21}+A_{21})}. \tag{2.16}$$

Note also that the nonscattering source term in (2.12) contains a contribution that depends on the collision coefficient C_{12} and approaches zero with Δt_n. It is also seen that the contribution of the nonscattering source term relative to the scattering source term decreases as Δt_n increases. The transport equation derived for the LTE version of the implicit Monte Carlo method displays similar properties [13].

Equation (2.12) gives a complete description of the radiation field in the time interval t_0 to $t_0+\Delta t_n$. The change in the atomic level populations can be determined using the principle that every photon absorbed results in the destruction of one lower state atom and the production of one upper state atom.

Integration of both sides of (2.12) over direction and frequency gives

$$\begin{aligned}\frac{\partial}{\partial t}\int_{-1}^{1} d\mu \int_0^{\infty} dv f(\mu, v, x, t)+\frac{\partial F}{\partial x}\\ =\gamma A_{21}(n(t_0)+\Delta t_n C_{12})-\int_{-1}^{1} d\mu \int_0^{\infty} dv c\sigma_a(v) f(\mu, v, x, t)\\ =\frac{\partial n_p}{\partial t},\end{aligned} \tag{2.17}$$

where F is the photon flux per unit atom density, and n_p is the photon density per unit atom. Integrating (2.17) over the duration of the integration cycle gives the following equation for the net change in the photon density per unit atom

$$\Delta n_p=\gamma A_{21}(n(t_0)+\Delta t_n C_{12})\,\Delta t_n-\int_{-1}^{1} d\mu \int_0^{\infty} dv \int_{t_0}^{t_0+\Delta t_n} dt c\sigma_a(v) f(\mu, v, x, t) \tag{2.18}$$

which is the difference between the photon weight per unit atom added by the sources and the total photon weight per unit atom absorbed. In the absence of collisions Δn_p could be taken as the negative of the change in the upper state population fraction, but in the presence of collisions, the upper state population must be updated with the help of (2.8).

3. The Monte Carlo Procedure

The Monte Carlo procedure for solving the coupled transport and atomic level population rate equations follows closely the procedure already developed for LTE problems. For explicit details regarding generation of source particles, geometry, and particle tracking the reader is referred to [13]. A brief summary of the procedure for line transport is given here.

Space is divided into fixed or variable width zones of width Δx. Atomic level populations are assumed to be constant over each zone. Photon sources are created in each zone with strength determined by the level population fraction $n(t_0)$ and the first right hand term in (2.12). Source photon bundles or particles are generated during each integration cycle and in each zone with weights appropriate to the source strength and the number of particles assigned to the zone. All photons are generated independently and are characterized by a position x within the zone, a time t within the integration cycle, and a randomly distributed direction cosine μ. A frequency is assigned on the basis of the normalized line shape distribution $\phi(\nu)$.

Photon bundles are followed to collision, boundary crossing, or census, whichever is appropriate. The direction and frequency of a particle are reassigned following each collision. Over each segment of path the photon weight is exponentially attenuated. At census the accumulated weight lost from the radiation bundles in each zone is used to raise atoms from the lower to the upper state in that zone in accordance with (2.8). Photon bundles that are reduced to an arbitrary fraction of their initial weight as well as those that exit from the system are terminated. Photon bundles that reach census are stored to be transported during the following cycle.

The frequent occurrence of scattering events makes it essential to pick frequencies from the line shape distribution $\phi(\nu)$ efficiently. The following scheme was designed to achieve this end.

The line shape profile of greatest interest and the one that we have considered is the Voight profile [1], which has been normalized to unity,

$$H(a, \nu) = \pi^{-1} \int_0^\infty e^{-[ax + (x^2/4)]} \cos(\nu x)\, dx. \tag{3.1}$$

Since this distribution is a symmetric function of ν, we need only consider positive values of ν. Integrating (3.1) over ν from 0 to ∞, we obtain the following expression for the cumulative distribution function on the half interval $(0, \infty)$,

$$F(a, \nu) = \frac{2}{\pi} \int_0^\nu e^{-[ax + (x^2/4)]} \frac{\sin \nu x}{x}\, dx. \tag{3.2}$$

On the interval $(0, \infty)$ N frequency bins, delimited by $\nu = 0, \nu_1, \nu_2, \ldots, \nu_{N-1}, \infty$ are determined by numerical integration such that the values of $F(a, \nu)$ occur in equal increments of $1/N$. When it is necessary to select a frequency from the distribution (3.1), one of the N intervals defined by the frequencies above is selected by taking the integer part of Nr, where r is a random number distributed uniformly on the interval (0, 1). The cross section for a photon bundle in the frequency interval (ν_i, ν_{i+1}) is set equal to the average of the appropriate cross section on the interval evaluated using (3.1) and (2.15). If the interval (ν_{N-1}, ∞) is selected, the photon cross-section is set to zero and the photon bundle is allowed to escape from the system.

The above procedure is equivalent to representing the distribution (3.1) as a histogram. In Fig. 1 and 2 we show a Voigt profile and its histogram approximation

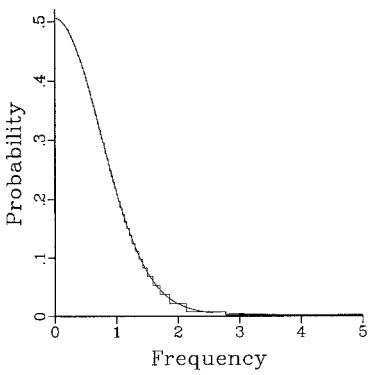

FIG. 1. Voigt profile for $a = 0.1$ and its 80 group histogram approximation.

for $N = 80$ and $N = 640$, respectively. With 640 frequency groups the Voigt profile is accurately represented even in the wing of the profile. Clearly the efficiency of the calculation, provided the initial investment of locating the frequencies v_1, v_2,..., v_{N-1} can be neglected, is independent of the number of requency intervals, and the latter should be influenced only by the available storage.

4. Evolution of a Simple Two-Level System to a Steady State

Since we know of no other method for solving the complete time-dependent line transport problem with collisions, we found it necessary to test the implicit Monte Carlo technique by comparing the steady-state solution reached asymptotically in a time-dependent calculation with the steady-state solution generated by a time-independent method [15]. We are indebted to W. E. Alley for providing the results obtained with this method [16].

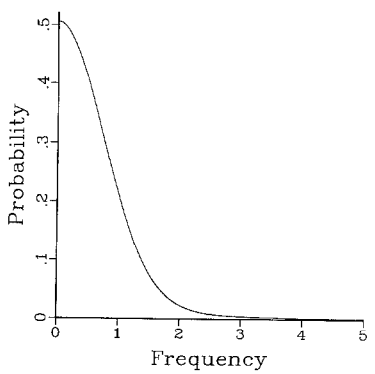

FIG. 2. Voigt profile for $a = 0.1$ and its 640 group histogram approximation.

TABLE I

The Physical Problem Parameters for Section 4

$n(x, t=0)$	0.25
$f(\mu, \nu, x, t=0)$	0.0
K_{21}	15.3422
K_{12}	15.3422
A_{21}	3.33564
C_{12}	0.245423
C_{21}	0.667128
a	0.0
Δt	0.2

Consider a slab of finite width open to a vacuum on both ends. Initially the upper level population fraction, n, is a constant function of position, and no photons are present. The system is pumped by collisions and evolves to a nontrivial steady-state. The parameters for the problem are given in Table I. Here time is measured in units of the time required for light to traverse the slab. A total of 640 frequency intervals were used to represent the line shape profile. About 1500 were used in the time-independent calculation [16].

The solution to (2.12) and (2.8) provides the radiation field and level populations as a function of position. Steady-state methods such as those described in [15], on the other hand, specify the solution as a function of optical depth. For this reason it was necessary to generate the implicit Monte Carlo solution first and then to map position onto optical depth. The two steady-state profiles of the upper level population fraction, plotted as a function of optical depth for the right half of the slab, are displayed in Fig. 3. The Monte Carlo values are generated at zone centers, and the steady-state calculation values are determined at zone boundaries. To minimize the effect of statistical fluctuations the Monte Carlo values of population fraction

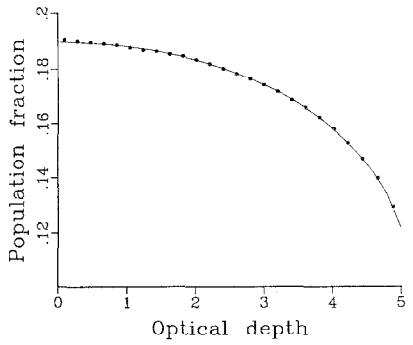

FIG. 3. Comparison of steady-state upper level population fraction calculated by implicit Monte Carlo and the steady-state method in [15].

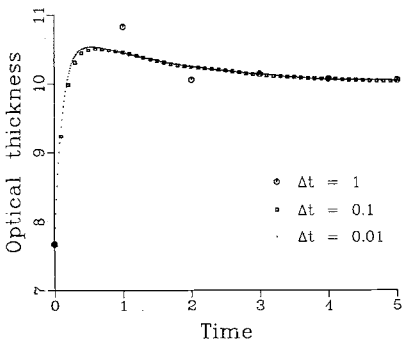

FIG. 4. Slab optical thickness as a function of time for different values of the integration time-step Δt.

were averaged over time from $t = 10$ to $t = 20$. The agreement between the two forms of calculation is seen to be excellent.

The approach of the system to steady state is shown in Fig. 4. Here the optical thickness of the slab as a function of time is plotted for three different choices of the time-step Δt. It is seen that regardless of time-step size the system reaches the correct asymptotic time behavior, indicating that the implicit Monte Carlo algorithm is stable for any choice of time-step.

Monte Carlo calculations were carried out for the parameter values in Table I and different numbers of frequency groups in the line. The convergence of the time-averaged slab optical thickness as a function of the number of frequency groups is indicated in Table II. Once we exceed 640 frequency groups the statistical error in the data masks the accuracy improvement coming from better frequency resolution. The particle population reached a steady-state number of approximately 50,000 particles. This rather large number is justified, however, by the accuracy implied in the values in Table II.

In Table III and Fig. 5 we show the sensitivity of the Monte Carlo steady state optical thickness and upper level population fraction to zone size. The convergence

TABLE II

Convergence as the Number of Frequency Groups Is Increased

N groups	Optical thickness
10	10.4967
20	10.1941
40	10.0759
80	10.0247
160	10.0051
320	10.0032
640	10.0004
1280	10.0027

TABLE III

Convergence as the Number of Zones Is Increased

N zones	Optical thickness
2	10.0523
4	10.0281
8	9.9943
16	10.0061
32	9.9887
64	10.0011

as the number of zones is increased is very rapid with statistical errors dominating once we have 8 zones or more. In Fig. 5 one can see the statistical fluctuations increasing as the number of zones is increased. As the number of particles in the slab was held fixed, the number of particles per zone decreases as the number of zones is increased. This causes the statistical errors in zonal quantities to increase with the number of zones.

5. Time-Dependent Radiation Trapping

We turn next to the description of the time-dependent diffusion of upper level excitation, which occurs, for example, following the irradiation of a gas by a pulsed

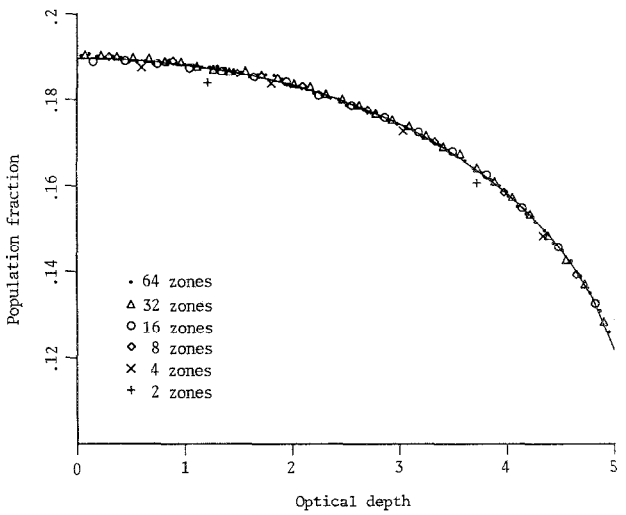

FIG. 5. Steady-state upper level population fraction calculated by implicit Monte Carlo for various zone sizes.

TABLE IV

The Physical Problem Parameters for Fig. 6

$n(x, t=0)$	$0.25\exp(-x^2/.02)$
$f(\mu, v, x, t=0)$	0.0
K_{21}	15.3422
K_{12}	15.3422
A_{21}	3.3356
C_{12}	0.0024
C_{21}	0.0067
a	0.0
Δt	$1/A_{21}$

laser beam [8]. Consider again a slab open at both ends with a Gaussian initial excited state population distribution. The parameters for the first problem are given in Table IV. The slab is approximately 15 optical depths in thickness.

In Fig. 6 we show the upper level population fraction as a function of distance from the center of the slab for the first 10 integration time-steps. The zoning is the same as for Fig. 3. In the absence of trapping and collisional pumping the excitation should everywhere drop to $1/e$ of its previous value after each integration step. The population actually drops less than 45% following the first time-step due to radiation trapping. In the last few time-steps the approach to the steady-state distribution established by collisions is evident.

In Fig. 7 we show the evolution in time of the same population distribution for the same slab size and the parameters in Table V. In this case the slab contains approximately 1200 optical depths. In Fig. 7 the upper state population fraction is plotted in increments of 10 integration steps. Due to the severity of the radiation trapping it takes approximately 80 spontaneous emission lifetimes for the population fraction at the center of the slab to decay to 50% of its starting value.

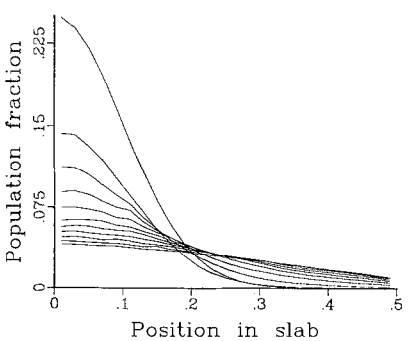

FIG. 6. Time-dependent diffusion of upper level population fraction as a function of time for a slab 15 optical depths in thickness.

TABLE V

The Physical Problem Parameters for Fig. 7

$n(x, t=0)$	$0.25\exp(-x^2/.02)$
$f(\mu, v, x, t=0)$	0.0
K_{21}	1885.0
K_{12}	628.33
A_{21}	.0165
C_{12}	10^{-8}
C_{21}	10^{-8}
a	0.031
Δt	$1/A_{21}$

6. Problem Running Times

The program was coded for a VAX 11/780 in the C programming language. Optically thin problems ran typically for about an hour, whereas optically thick problems ran for approximately 30 h. This would translate, roughly, to a fraction of a minute and 20 min. of equivalent Cray 1 running time. It should be emphasised, however, that no attempt was made to optimize the efficiency of the calculation through particle number control or other methods, since our primary interest was in demonstrating the stability and accuracy of the underlying method.

The use of random walk methods similar to those employed in the LTE application of implicit Monte Carlo [14] could be expected to greatly improve the efficiency of the calculation in zones of high opacity. On the other hand, for problems that involve large numbers of scatters, the addition of extra dimensions would not be expected to add greatly to the problem running time for slabs.

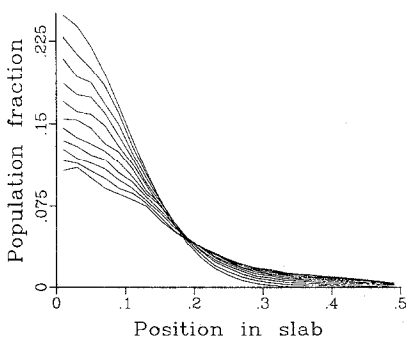

FIG. 7. Time-dependent diffusion of upper level population fraction as a function of time for a slab 1200 optical depths in thickness.

7. Summary and Conclusions

We have derived an implicit Monte Carlo technique applicable to two-level time-dependent line transport with collisions. We have demonstrated that the stability of the method is independent of the size of the integration time–step over a range of time-step sizes that span any characteristic time scale of the system. We have tested the accuracy of the method by comparing the asymptotic steady-state generated in a time-dependent problem with the solution generated with the help of a conventional steady-state method. The two methods of solution were found to be in excellent agreement. We have also demonstrated that the method is applicable to optically thin or optically thick media. The most promising applications for the implicit Monte Carlo line transport methods should be those that involve complex scattering models, multidimensional geometry, or both.

References

1. D. Mihalas, *Stellar Atmospheres* (Freeman, San Francisco, 1978).
2. G. Bekefi (Ed.), *Principles of Laser Plasmas* (Wiley, New York, 1976).
3. T. Holstein, *Phys. Rev.* **72**, 1212 (1947), **83**, 1159 (1951).
4. M. G. Payne and J. D. Cook, *Phys. Rev. A* **2**, 1238 (1970).
5. C. Van Trigt, *Phys. Rev. A* **13**, 734 (1976).
6. A. G. Zajonc and A. V. Phelps, *Phys. Rev. A* **23**, 2479 (1979).
7. T. Fujimoto and A. V. Phelps, *Phys. Rev. A* **25**, 322 (1982).
8. W. Molander, M. Belsey, A. Streater, and K. Burnett, *Phys. Rev. A* **29** (1984).
9. P. B. Kunasz, *Ap. J.* **271**, 321 (1983).
10. W. E. Alley, *J. Quant. Spectrosc. Radiat. Transfer* **30**, 571 (1983).
11. L. W. Avery and L. L. House, *Ap. J.* **152**, 493 (1968).
12. L. H. Auer, *Ap. J.* **153**, 783 (1968).
13. J. A. Fleck, Jr. and J. D. Cummings, *J. Comput. Phys.* **8**, 313 (1971).
14. J. A. Fleck, Jr. and E. H. Canfield, *J. Comput. Phys.* **54**, 508 (1984).
15. E. Averett, *J. Quant. Spectrosc. Radiat. Transfer* **11**, 519 (1971).
16. W. E. Alley, Private communication.